Fire behavior of innovative alginate foams

Thierry Vincent, Chloë Vincent, Loïc Dumazert, Belkacem Otazaghine, Rodolphe Sonnier, Eric Guibal

Fire behavior of innovative alginate foams

Thierry Vincent, Chloë Vincent, Loïc Dumazert, Belkacem Otazaghine, Rodolphe Sonnier, Eric Guibal *

IMT – Mines Ales, Polymers Hybrids and Composites (PCH), 6 Avenue De Clavières, F-30319 Alès Cedex, France

A B S T R A C T

A new biosourced composite foam (AF, associating foamed alginate matrix and orange peel filler) is successfully tested for fire-retardant properties. This material having similar thermal insulating properties and density than fire-retardant polyurethane foam (FR-PUF, a commercial product) shows promising enhanced properties for flame retardancy, as assessed by different methods such as thermogravimetric analysis (TGA), pyrolysis com-bustion flow calorimetry (PCFC) and a newly designed apparatus called RAPACES for investigating large-scale samples. All these methods confirm the promising properties of this alternative material in terms of fire pro-tection (pHRR, THR, EHC, time-to-ignition, flame duration or production of residue), especially for heat flux not exceeding 50 kW m^{-2}. At higher heat flux (i.e., 75 kW m^{-2}), flame retardant properties tend to decrease but maintain at a higher level than FR-PUF. The investigation of the effect of AF thickness shows that the critical thickness (CT) is close to 1.5–1.7 cm: heat diffusion and material combustion are limited to the CT layer that protects the underlying layers from combustion. A multiplicity of factors can explain this behavior, such as: (a) negligible heat conduction, (b) low heat of combustion, (c) charring formation, and (d) water release. Water being released from underlying layers, dilutes the gases emitted during the combustion of superficial layers and promotes the flame extinction.

Keywords:
Alginate
Composite material
Thermal insulation foam
Fire behavior
Radiant panel

1. Introduction

Polymeric foams are extensively used in industry in various sectors such as building, transport, packaging, furnishing, etc. In 2018, the global market for these materials reached up to USD 109.71 billion, and its annual growth rate is estimated at 4 % for the next 7 years (Grandviewresearch, 2019). Producing light materials with thermal insulating properties is a challenge for these industrial sectors. For some of these applications, bringing flame retardancy properties is of critical importance. Therefore, many recent studies were carried out to design new flame retardant foams. Most of this research focused on synthetic-based foams using polyolefins (Huang et al., 2019), poly(lactic acid) (Vadas et al., 2018), phenol (Delgado-Sanchez et al., 2018; Mougel, Garnier, Cassagnau, & Sintes-Zydowicz, 2019), melamine (Yang, Cao, Wang, & Schiraldi, 2015), polystyrene (Wang, Zhao et al., 2018; Hamdani-Devarennes et al., 2016), and polyurethane (Carosio, Negrell-Guirao, Alongi, David, & Camino, 2015; Chen et al., 2018).

Many polymers have intrinsic high flammability due to their proper chemical composition and structure. However, in the case of polymeric foams this flammability is even increased due to a couple of specific phenomena. First, the foams have a low thermal conductivity. This means that heat cannot be efficiently transferred from exposed surface

Abbreviations: AF, Alginate foam (with incorporation of orange peel); CHF, Critical heat flux (kW m^{-2}); C_p, Specific heat (J kg^{-1} K^{-1}); CT, Critical thickness (cm); E_d, Young modulus for compression test (MPa); EHC, Effective heat of combustion (kJ g^{-1}); EPS, Expanded polystyrene foam; FIGRA, Flame index growth rate (kW m^{-2} s^{-1}); F_G, F_M,F_{MM}, F_{GM},F_{GG}, Fractions of mannuronic acid and guluronic acid moieties and assemblies in alginate; FR-PUF, Fire-retardant polyurethane foam; FTIR, Fourier transform infra-red spectroscopy; HRR, Heat release rate (W g^{-1} for PCFC analysis, kW m^{-2} for RAPACES test); K, Heat or thermal conductivity (W m^{-1} K^{-1}); l, Thickness (m in Eq. 2, or cm); NMR, Nuclear magnetic resonance; OP, Orange peel; PCFC, Pyrolysis combustion flow calorimetry; pHRR, Peak of HRR (W g^{-1} for PCFC analysis, kW m^{-2} for RAPACES test); PU, Polyurethane foam; Py-GC–MS, Pyrolysis-gas chromatography-mass spectrometry; $\ddot{q}_{ext}$, External heat flux (kW m^{-2}); RAPACES, RAdiant PAnel Concentrator Experimental Setup; SEM, Scanning electron microscopy; SEM-EDX, SEM-coupled energy dispersive X-ray analysis; SLS, Sodium lauryl sulfate; T, Temperature (°C or K); T_{ig}, Temperature at ignition (°C or K); TGA, Thermogravimetric analysis; THR, Total heat release (kJ g^{-1}); TTI, Time-to-ignition (s); UL94, UL 94 flammability classification (V grade); w_R, Water regain (%); ε, Emissivity; [η], Intrinsic viscosity (dL g^{-1}); ρ, Density or apparent volumetric mass (dimensionless or kg m^{-3}, resp.); σ_{10}, Compression strength at 10 % deformation (MPa).

* Corresponding author.
E-mail address: Eric.Guibal@mines-ales.fr (E. Guibal).

to the bulk of the material. This property is promoting the fast ignition of the surface of the foam. In addition, rapidly the material tends to shrink, which, in turn, leads to the collapse of the porous structure of the foam and to the formation of a pool fire (Krämer, Zammarano, Linteris, Gedde, & Gilman, 2010; Wang et al., 2019). Oxidative processes, especially in the case of open-cell foams, reinforce these effects. The density of the foam strongly influences shrinkage and heat release rate (Wang et al., 2019). Rigid and flexible PU (polyurethane) foams, as well as expanded polystyrene (EPS) foams, have very interesting and adaptable properties that may explain their large application in packaging; however, these PU foams are hazardous in terms of fire propagation. Indeed, they release huge heat amounts during combustion, together with black and toxic smokes. Although some bio-based alternatives have been recently documented, especially for PU (Agrawal, Kaur, & Walia, 2017; El Hage et al., 2019), most of these materials are petro-sourced.

Different strategies have been proposed for limiting the flammability of flexible or rigid PU foams:

a) incorporation of phosphorus flame retardant reactive groups; including in some cases bio-based compounds (Chen et al., 2018; Ding et al., 2017; Li, Wang, Chen, Shi, & Hao, 2019; Lorenzetti et al., 2013; Rao et al., 2018; Tian, Yao, Zhang, Wang, & Xiang, 2018; Wang, Wang et al., 2018; Yang, Wang, Han, Ma, & Li, 2017; Zhang, Pan, Zhang, Hu, & Zhou, 2014) or additives (alone or combined with synergists) (Realinho, Haurie, Formosa, & Ignacio Velasco, 2018)
b) addition of fillers (Wang et al., 2017; Yang et al., 2019), or
c) coating (Carosio et al., 2015; Carosio, Ghanadpour, Alongi, & Wagberg, 2018; Li et al., 2020; Mu et al., 2017; Pan et al., 2019).

The toxicity of the smokes produced during the combustion of PU or EPS is an important criterion not only for fire management but also for their life cycle (final elimination). Their poor biodegradability makes these widely-dispersed materials important sources for long-time contamination of the environment. There is a need for developing alternative materials being more environmentally friendly both in terms of life cycle (production, service-life and end-of-life) but also in terms of management of non-renewable resources. Recently, several studies have been reported on the substitution of petro-sourced compounds with bio-based resources for the synthesis of light, insulating materials with good fire-retardant properties (Agrawal et al., 2017). Alginate, among other polysaccharides or other bioresources (Jones et al., 2018; Jones, Mautner, Luenco, Bismarck, & John, 2020), has retained a great attention for the last decade for developing innovative materials (Simkovic, 2013). Alginate is a polysaccharide constituted of α-L-guluronic acid and β-D-mannuronic acid units (Draget, SkjakBraek, & Smidsrod, 1997), which can be ionotropically gelled in the presence of various metal cations (Agulhon, Robitzer, Habas, & Quignard, 2014). This fundamental property was used for designing different shapes of alginate gels such as beads, fibers (Jeon, Bouhadir, Mansour, & Alsberg, 2009; Qin, 2008; Zhang, Xia, Yan, & Shi, 2018), films (Hou, Xue, & Xia, 2018), or foams (Gady, Poirson, Vincent, Sonnier, & Guibal, 2016; Li, Chen, & Chen, 2019; Vincent et al., 2018). Alginate was also used for preparing fire-retardant layer-by-layer coatings (Mu et al., 2017; Pan et al., 2019). It is noteworthy that alginate burning releases less than 3 kJ g^{-1} while heat release usually ranges between 10 and 44 kJ g^{-1} for most common polymers. This is an obvious justification of the interest of alginate for elaborating fire-retardant foams.

Actually, the different studies discussing the fire-retardant properties of alginate-based materials have shown that flammability strongly depends on the metal used for alginate ionotropic gelation. For the last decade, several studies have compared the fire properties of alginate-based supports where the biopolymer was gelled using iron (Liu et al., 2016a; Liu et al., 2014a), aluminum (Liu, Li et al., 2015), nickel, copper (Liu, Zhao et al., 2015), zinc (Liu, Zhao, Zhang, Ji, & Zhu, 2014; Liu et al., 2016b), calcium (Zhang et al., 2011), barium (Liu et al., 2016c; Zhang, Ji, Wang, Tan, & Xia, 2012), manganese, cobalt (Liu et al., 2016d). Figure AM1 (see Additional Material Section, AMS) shows the plot of flammability rating of different alginate-metal compounds (according to the UL94 test of fire propagation) as a function of their limit oxygen demand index (LOI). Many of the couples "alginate/metal ion" (including Ca(II), Fe(III), Al(III), Co(II), Zn(II), Ni(II) and Ba(II)) have (a) LOI superior to 30 (i.e., low flammability; compared with the 21% ratio of oxygen in air), and (b) V0 rate in the UL 94 test (negligible fire propagation).

The objective of the study focuses on the comparison of the flammability properties of a low-density alginate-based foam with a reference commercial material (i.e., a flame retardant polyurethane foam having similar thermal insulation properties, FR-PUF). These fire-retardant properties are compared using different analytical tools such as TGA (thermogravimetry analysis), PCFC (pyrolysis combustion flow calorimetry). In addition, a new equipment (called RAPACES) was also used for the evaluation of thermal degradation of larger samples (bench scale). This original equipment allows testing surfaces as large as 20 × 20 cm (in this study; though samples of larger size can be also tested).

2. Materials and methods

2.1. Materials

Alginate was supplied by FMC BioPolymer (Philadelphia, PA, USA). Water content in the biopolymer sample was determined by a thermogravimetry analyzer (PerkinElmer TGA 4000, Waltham, MA, USA) using N_2 as the analysis atmosphere and a temperature ramp of 10 °C min^{-1}. The characteristics of the biopolymer were determined by ^{13}C NMR spectroscopy and viscosimetry for the determination of the mannuronic acid/guluronic acid molar ratio (M/G, and structural properties) and the molecular weight, respectively. ^{13}C NMR was performed on a Bruker Avance 400 (Billerica, MA, USA), after conditioning the sample in D_2O at 80 °C (Grasdalen, Larsen, & Smidsrod, 1979; Grasdalen, Larsen, & Smidsrod, 1977). The molecular weight ($\overline{M_v}$, kDa) was deduced from the intrinsic viscosity ([η], dL/g) (measured using Ubbelohde viscosimeter) and the Mark-Houwink-Sakurada equation (Torres et al., 2007), $[\eta] = 0,023\ \overline{M_v}^{0,984}$.

The average molecular weight was 446,000 Da (corresponding to an intrinsic viscosity of 931 dL g^{-1}). The water content was close to 16.3 % and the M/G ratio was evaluated to 0.19 (F_M : 0.159, F_G : 0.841 ; F_{MM} : 0.342, F_{GM} : 0.342, F_{GG} : 0.499).

Orange peels were dried at 50 °C before being grinded and sieved to 250 μm. Sodium lauryl sulfate (SLS) was provided by Merck KGaA (Darmstadt, Germany); anhydrous calcium carbonate was supplied by Prolabo (Fontenay/bois, France), and Gluconolactone by Sigma-Aldrich (Lyon, France). All chemical reagents were analytical grade (>99%). Alginate contained less than 3% impurities (ashes).

The commercial flame-retardant PU foam (FR-PUF) was kindly provided by SOPREMA (Strasbourg, France). Figure AM2 shows the SEM-EDX analysis of the FR-PUF that contains elements C, N, O elements associated with the PUF, but also elements such as Cl, P that are tracers of the fire-retardant adjuvant; Si and K are probably surface impurities. SEM-EDX were recorded using an environmental scanning electron microscope Quanta FEG 200 (FEI France, Thermo Fisher Scientific, Mérignac, France), equipped with an Oxford Inca 350 energy dispersive X- ray micro-analyzer (Oxford Instruments France, Saclay, France). SEM was also used for characterizing the morphology of the foams (under an acceleration voltage of 12.5 keV).

2.2. Synthesis of alginate foam

The synthesis procedure is based on the concept of alginate foaming (using SLS) followed by controlled ionotropic gelation (modulating gelling with calcium salt and gluconolactone) (Vincent et al., 2018). The

incorporation of an organic filler (orange peel) contributes to slightly strengthening the foam, giving additional hydrophilic behavior and improving mechanical properties.

Alginate was dissolved in demineralized water to prepare a 4% (w/w) solution; SLS solution (1%, w/w) was prepared by dilution in demineralized water. After calcium carbonate dispersion in water, the 10% (w/w) suspension of $CaCO_3$ was maintained under agitation until use.

The synthesis procedure includes four steps (Scheme AM1, see Additional Material Section). First, the different ingredients were mixed under strong agitation: 640 g of the alginate solution (4%, w/w), 20 g of orange peel, 20 g of $CaCO_3$ suspension (10%, w/w), 20 mL of SLS solution (1%) and 350 g of demineralized water for 30 min. In the second step, 12 g of gluconolactone were added under agitation to the foaming solution for 1.5 min. The third step consisted of pouring the foam into a mold. At the fourth step, the foam (AF) was dried in an oven at 35 °C for 4 days. AF foams without incorporation of orange peel (AF wo peel) were also produced with the same process.

Experimental conditions can be varied to produce foams of increasing density (Vincent et al., 2018). For the current study, the formulation was adapted to reach a density (i.e., 40 kg m^{-3}) close to the value reported for commercial sample FR-PUF (i.e., 43 kg m^{-3}). Indeed, foam density is a critical parameter for the burning behavior associated with shrinkage phenomena and heat release rate (Wang et al., 2019). Choosing foam blocks of similar density is necessary for effective comparison of the two materials (i.e., AF and FR-PUF).

For evaluating the critical thickness, Alginate Foams (AF) were produced varying the volume/mass of foam disposed in the mold. The effective thicknesses of the mono-blocks were 1.0, 1.2, 1.7 and 2.1 cm. For preparing multilayer foam blocks (increasing the thickness of AF up to 3 cm) several thin AFs were glued with alginate solutions (Figure AM3).

2.3. Characterization of materials

2.3.1. Previous characterization

Table 1 reports some characteristics of the two materials: dimensions (for bench scale tests), density, thermal conductivity (K, W m^{-1} K^{-1}) and specific heat (C_p, J kg^{-1} K^{-1}). The thermal conductivity was measured using the transient hot-wire thermal conductivity method (NEOTIM FP2C, NEOTIM, Albi, France) with the following experimental conditions: 0.5 s sampling time; 0.04 W source power; 10.7 Ω resistance and 130 s analysis duration. The thickness of the samples was 1.3 cm for AF and 3.5 cm for FR-PUF. The specific heats were determined using a Diamond differential scanning calorimeter (PerkinElmer, Waltham, MA, USA). Analyses were performed on 5-mg samples using the Step Scan mode. A first step consisted of a 2-min isotherm at 0 °C (under N_2 flow – 20 mL min^{-1}) followed by 40 successive steps of 1 min at increasing temperatures (1 °C at each step) and isotherm measurement for 1 min.

Table 1
Main characteristics of Alginate and FR-PU foams.

Criteria	Alginate foam	FR-PU foam (BING, 2006; Yang, Yi, Liu, & Zhao, 2016; Zhang, Liu, Chen, Wang, & Song, 2015)
Dimensions (surface, @ benchscale, cm)	20 × 20	10 × 20
Thickness[a] (cm)	1.7 – 2.1 – 3.0	1.0 – 1.2 – 2.0
Density (kg m^{-3})	40	43
Thermal conductivity (k, W m^{-1} K^{-1})	0.03	0.02
Specific heat (C_p, J kg^{-1} K^{-1})	1600	1160

[a] for alginate foams, the thickness @ 3 cm was obtained as a multilayered material (two layers glued together; alginate solution being used for binding the two foams).

2.3.2. X-ray diffraction analysis (XRD)

X-ray diffraction (XRD) data (on powders) were collected using a BRUKER Advance D8 diffractometer in a θ–θ configuration employing Cu K_a radiation (λ=1.54 Å) with a fixed divergence slit size of 0.3 and a rotating sample stage. The samples were scanned between 10° and 70° with a VANTEC-1 detector. The qualitative analysis was performed with the X'Pert High Score Plus software (version 2.1).

2.3.3. Thermogravimetry analysis (TGA)

TGA spectra were obtained using a Pyris 1 thermogravimetric analyzer (PerkinElmer, Waltham, MA, USA). A fixed amount of material (i.e., 10 ± 0.2 mg) was heated under nitrogen flow (at 20 mL min^{-1}) applying a temperature ramp of 10 °C min^{-1}, from ambient to 900 °C. A 2-min isotherm step was processed at 30 °C.

2.3.4. Pyrolysis combustion flow calorimetry (PCFC)

Fuel production was recorded using a pyrolysis combustion flow calorimeter (PCFC, Fire Testing Technology, East Grinstead, UK), developed by Lyon and Walters (Lyon & Walters, 2004). A fixed amount of sample (i.e., 3 ± 0.5 mg) was heated at a rate of 1 °C s^{-1} under nitrogen atmosphere (flow: 100 mL min^{-1}) from 80 to 750 °C. The products of the degradation were transferred to a combustion chamber where they are mixed with an excess of oxygen at 900 °C. Under these conditions (usually referred as Method A in ASTM D 7309 (ASTM, 2013)), these products can be considered fully oxidized. The Heat release rate (HRR) was calculated by oxygen depletion according to Huggett relationship (Huggett, 1980): 1 kg of consumed oxygen corresponds to 13.1 MJ of released energy. The solid residue was also pyrolyzed (according the so-called Method B; i.e., under aerobic atmosphere – 20% oxygen) and the gaseous products were burnt in the combustion chamber under conditions similar to Method A. The experimental conditions are similar to those reported for anaerobic pyrolysis, except that nitrogen flow is replaced with airflow in pyrolyzer.

2.3.5. RAPACES testing

A new analytical tool (RAPACES, Radiant Panel Concentrator Experimental Setup) was recently designed at IMT Mines Ales for the study of fire properties of samples of larger size than those analyzed by the cone calorimeter method (Vincent et al., 2015; Vincent, 2016) (Figure AM4). The same parameters can be measured (mass loss rate, heat release, etc.). This equipment allows applying a scale factor as high as 10 compared with cone calorimeter and the mode of irradiation can be changed (horizontal *vs.* vertical exposure) (Figure AM4). Briefly, the radiative heat source consists of two 60 kW panels with a total emitting surface of one m^2 corresponding to a maximum emitted heat flux of 120 ± 2 kW/m^2 (Chaudelec, Brignais, France). Each panel is equipped with a series of 3 kW short-wave infrared (IR) tungsten lamps with a color temperature of 2400 K and a maximum radiation at a wavelength of ~ 1.2 μm. Four polished stainless steel plates constitute a tunnel between the source and the sample to concentrate the radiative heat flux towards the sample compartment. A calibration test was performed applying a heat flux of 80 kW m^{-2}. A CAPTEC radiative flux meter (Lille, France) confirmed that the distribution of the heat flux received at the surface of the sample was nearly homogeneous. Received heat flux varied between 78 and 82 kW m^{-2} on a 40 cm × 40 cm surface. Weight loss was monitored as a function of time (measurement frequency: 0.1 s) using a KERN weighing scale (Kern & Sohn GmbH, Balingen, Germany; 0−20 kg ±0.05 g). A SERVOMEX 4100 series gas analyzer (Servomex, Spectris Group, Egham, UK) was used for quantifying the concentrations of O_2, CO_2 and CO during the combustion test. These data were collected to calculate the HRR according the Huggett relationship. In this study, the samples were disposed in the horizontal position and the radiative flux was varied (i.e., 35, 50 and 75 kW m^{-2}). An electrical spark (placed at 1-cm distance from sample surface) initiated the combustion step. Each test was repeated three times to evaluate the repeatability. Type K thermocouples (with measurement range up to 1200 °C) were used for

measuring the surface temperature.

2.3.6. Pyrolysis-gas chromatography-mass spectrometry (Py-GC/MS)

The Py-GC/MS analytical setup consisted of an oven pyrolyzer connected to a gas chromatography/mass spectrometry system. A Pyroprobe 5000 apparatus (from CDS Analytical, Oxford, PA, USA) was used to pyrolyze the samples. One coil probe enables the samples heat in a helium environment. Each sample (less than 1 mg) was placed in a quartz tube between two pieces of quartz wool and was heated using an electrically heating platinum filament. The samples were successively heated at 300 °C and 700 °C. Each temperature was held for 15 s before gases were drawn to the gas chromatograph for 5 min. The pyrolysis interface was coupled to a 450-GC gas chromatograph (from Varian, Agilent, Palo Alto, CA, USA) by means of a transfer line heated at 270 °C. In this GC, the initial temperature of 70 °C was held for 0.2 min, and then raised to 310 °C at 10 °C/min. The column for separation was a Varian Vf-5 ms capillary column (30 m × 0.25 mm) and helium (1 mL/min) was used as the carrier gas; the split ratio was set to 1:50. The gases were introduced from the GC transfer line to the ion trap analyzer of the 240-MS mass spectrometer (from Varian, Agilent, Palo Alto, CA, USA) through the direct-coupled capillary column. Identification of the products was achieved comparing the observed mass spectra to those of the NIST mass spectral library (NIST, Gaithersburg, MD, USA).

2.3.7. Mechanical properties – compression tests

Compression tests were carried out on Zwick Z010 press equipped with a 10 kN sensor (ZwickRoell, Ulm, Germany). The sample was preloaded at 50 N (at 7 mm/min), while the test was performed with a 10 %/min strain speed. The test was stopped at rupture or after registering a 50% strain.

2.3.8. Water regain under controlled atmosphere

The water regain under humid atmosphere was approached using a simple mass-variation method. The pieces of foam (~6.91 g for AF and 5.77 g for AF without peel; dimensions: 85 × 100 × 20 mm for AF and 85 × 100 × 15 mm for AF without peel) were first dried in an oven at 50 °C for 72 h, before being stored for 24 h in a desiccator. The samples were exposed to a 75% humidity/25 °C atmosphere (saturated NaCl solution) in a closed chamber for 3 days. The weight-time curve was obtained by regularly weighing the pieces of foams.

2.3.9. Foam durability

Degradation tests were carried by determination of COD and BOD_{28}. COD measurements were performed on Hach DR 2000 (Hach Company, Ames, IO, USA) using the reactor digestion method (dichromate method; derived from USEPA Standard Method 5220 D); the foam was grinded before being digested. The BOD_{28} was determined by the manometric respirometry test, derived from the OECD Guideline 301 F using an OxiTop® IS-6 system (WTV, Xylem Analytics, Weilheim, Germany) after 28-days degradation time.

3. Results and discussion

3.1. Characterization of foam structure

3.1.1. Foam morphology – SEM

The SEM microphotographs (Fig. 1) show the morphology of the porous network for AF with (AF) and without (AF without OP) orange peels, at different magnitudes. The incorporation of orange peel hardly affects the aspect of the foams; the main change is appearing at the highest magnitude with less smooth scaffold surfaces. More generally, the texture of the foams may be characterized as scaffold constituted by irregular cells, which are not interconnected with thin scaffold walls (about 1−5 μm thick). The size of these pores is difficult to quantify, due to the shape irregularities, but these pores mostly range between 100 μm and 500 μm.

3.1.2. XRD characterization

The XRD analysis of the foams (with and without orange peels) are reported in Fig. 2 Mainly constituted of alginate (and when relevant orange peel), the foams are poorly crystalline, as confirmed by the poorly-resolved XRD patterns. However, the structure appears more

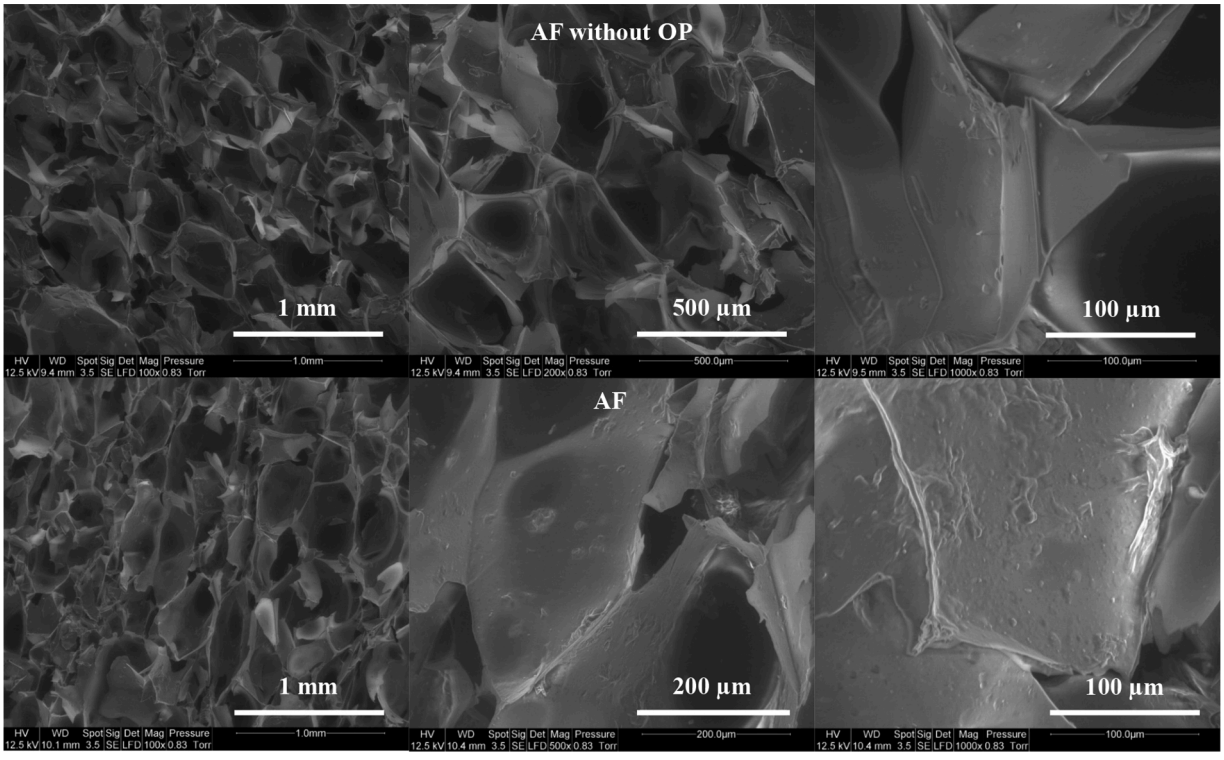

Fig. 1. SEM micrographs of AF with and without orange peel (at different magnitudes).

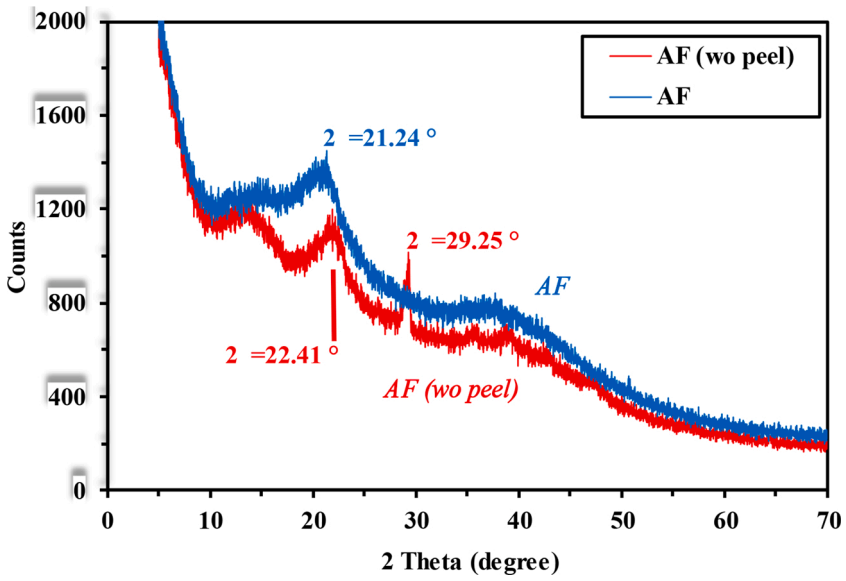

Fig. 2. XRD diffraction patterns AF with and without orange peel (wo peel).

crystalline than tannin-incorporated calcium alginate beads, where Sun, Zhang, Ding, and You (2020)) did not detect meaningful peaks.

The two materials are characterized by three peaks at 2θ ~ 14°, 21–22 ° and 36–38 °. These weakly-resolved peaks have also been reported by Sui et al. (2012). They assigned the scattering peak at 2θ = 13.5° to lateral packing among molecular chains (1 1 0), while the peak at 2θ = 21.5° was attributed to the layer spacing along the molecular chain direction (0 0 2). The third shoulder was not discussed. It is noteworthy that the AF without orange peel is also characterized by a well-marked peak at 2θ = 29.25° that disappears with the incorporation of orange peel. This peak may be correlated to the (1 0 4) diffraction plane of calcium carbonate identified on calcite (Kontoyannis & Vagenas, 2000). This interpretation is confirmed by the presence of small poorly-resolved peaks at 2θ ~ 33°, 36°, 39° and a shoulder at ~ 43°; other weak peaks reported by Kontoyannis and Vagenas (2000) are masked here by the amorphous background (double peaks in the range 2θ ~ 47–49 °, and 56–58 °). Apparently, the incorporation of orange peel masked the calcium carbonate contribution or the experimental conditions reduce the proportion of calcium salt in the final foam.

3.2. *Fire properties at microscale*

The thermal properties of the materials are compared under different conditions (anaerobic pyrolysis and combustion) using both TGA and PCFC (Fig. 3).

3.2.1. *TGA*

Fig. 3a shows the comparison of TGA profiles for FR-PUF, Alginate Foam, alginate powder and orange peel powder. The decomposition of FR-PUF occurs according three successive steps:

a) Beginning at 150 °C, the material loses about 10% of its weight.
b) Between 300 °C and 350 °C, the main decomposition corresponds to a weight loss of about 40%.
c) Between 350 °C and 950 °C, the material progressively (and slowly) loses about 24% of its weight: the residue finally represents about 26% of initial weight.

The derived curve for weight loss against temperature (not shown) identifies the maximum weight loss at 364 °C.

In the case of polyurethane (without incorporation of flame retardant), the decomposition of PUF was described as a two-step process, corresponding to (a) the decomposition of urethane and urea groups from diisocyanate, and (b) the decomposition of the polyether (Krämer et al., 2010). The decomposition strongly depends on the composition of the PUF (including the introduction of fire retardant compounds). However, Krämer et al. (2010) suggested that the thermal stability of compounds in the PUF follows the order: biuret ≈ allophanate < urethane < urea. The first two compounds degraded above 110 °C, while urethane and urea require higher temperatures (above 200 °C). This could correspond to the two weak waves observed in the range 150−250 °C. They also reported that the decomposition of urethane and urea leads to the formation of diisocyanate that is rapidly converted to diamino toluene. Simultaneously to these degradation steps, the polymeric structure is degraded: the structured material converted to a viscous liquid phase. Above 300 °C, the polyether moieties are degraded and volatile compounds are formed. Zhao, Nam, Richards, and Lekakh (2019)) reported three steps in the decomposition of PUF corresponding to: (i) the reverse formation of urethane groups with formation of isocyanate and alcohol, (ii) the dissociation to produce amine, carbon dioxide and olefins, and (iii) the dissociation to form secondary amine and carbon dioxide.

Obviously, in the case of FR-PUF, the incorporation of flame-retardants induces more complex thermal changes. A second reason for the difficulty in interpreting the TGA may consist of the occurrence of thermo-oxidative secondary phenomena associated with the diffusion of oxygen contained in the porous network. Even when the test is performed under nitrogen flow, air may be present in closed cells.

In the case of pure alginate (analyzed as powder), the biopolymer loses about 14% of its weight at 100 °C (corresponding to water release). An additional loss of weight (about 5%) is observed till 210 °C (release of structural water) before observing a strong and steep weight loss (about 30%) up to 280 °C. Between 280 °C and 530 °C, the weight loss linearly decreases by 12% (residue around 38%). The weight stabilizes up to 697 °C before the degradation of the char; the residue represents 15% at 900 °C. Roughly similar trends were reported by Safaei, Taran, and Imani (2019)), who commented successively the disappearance of absorbed and superficial water (below 150 °C), the volatilization of compounds (including water tightly bound to organic groups), the destruction of carboxyl groups and partial depolymerisation (below 450 °C) and the carbonization and complete removal of organic compounds (up to 800 °C).

Orange peel (OP) was included in the formulation of Alginate Foams. OP is mainly constituted of pectin (about 42%), cellulose/hemicellulose

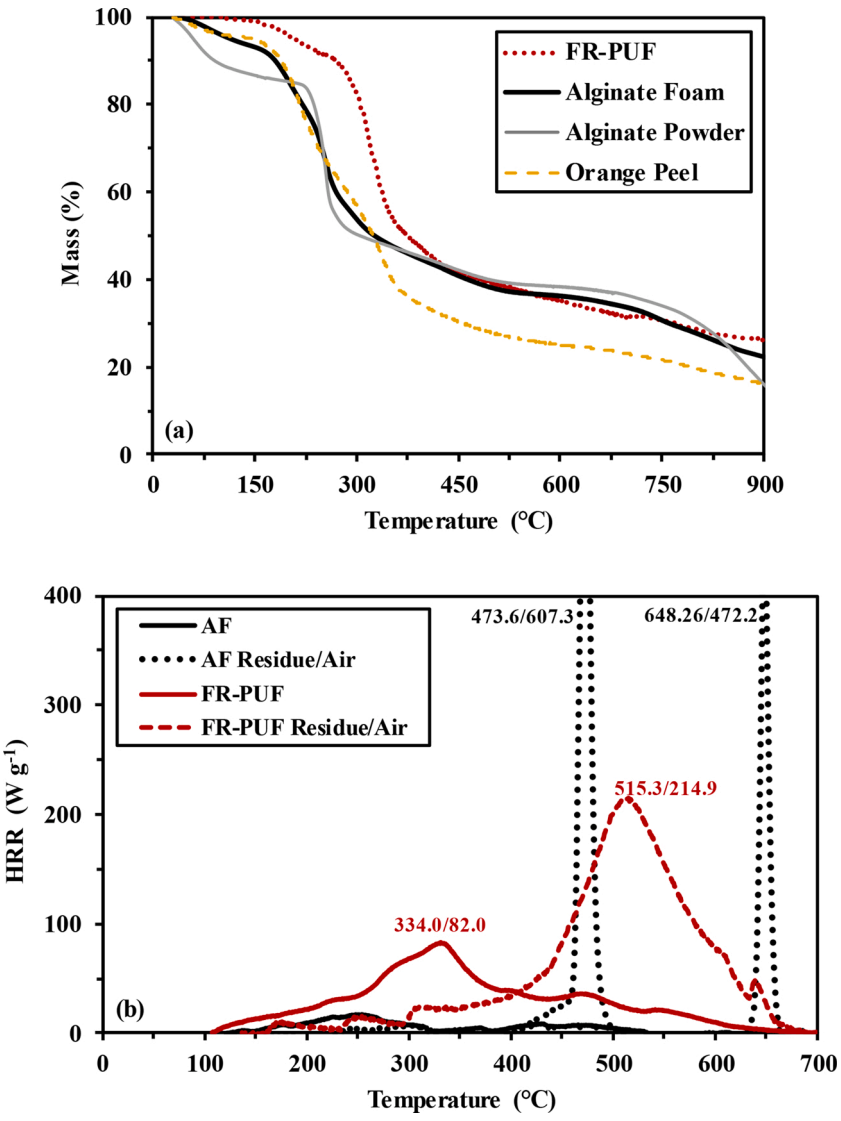

Fig. 3. Fire properties at microscale for AF and FR-PUF – (a) TGA curves, and (b) PCFC, HRR *vs.* Temperature for Alginate Foam (AF) and PUF (Anaerobic pyrolysis and aerobic pyrolysis of residues).

fraction (about 20%), sugars (about 17%) proteins (about 6.5%) (in addition to traces of lignin and ashes – about 0.8% and 3.5%, respectively) (Pathak, Mandavgane, & Kulkarni, 2017). The TGA profile is consistent with the results reported by Pathak et al. (2017): below 200 °C, water and volatile organic compounds (essential oils etc.) are released (this fraction represents about 10% weight loss). Between 200 and 250 °C, the pectin and hemicellulose fractions are decomposed (weight loss close to 25−30%). Another decomposition peak is reported between 300 °C and 400 °C (consistently with present results); this is associated with cellulose degradation (about 25−30%). The final residue represents between 20% and 25%. The derivative curve shows two peaks (maximum degradation rate) at 212 °C and 338 °C (consistently with Pathak et al. (2017)).

In the case of composite AF, TGA profile is similar to the profile obtained with FR-PUF with two weight-loss steps representing 10% and 40%; however, the profiles are shifted toward lower temperatures: the first weight loss occurs below 210 °C while the second is observed at temperature lower than 300 °C. The TGA profiles are roughly superimposed for AF and alginate powder: the incorporation of orange peels and other compounds during the synthesis (such as the foaming agent or the ionotropic gelation agent) does not change the thermal degradation behavior. The derivative curves (not shown) allow identifying a main peak at 251 °C and smaller peak at 199 °C. These results confirm the lower thermal stability of AF compared with FR-PUF while the incorporation of "additives" (including peel filler) does not significantly change the thermal stability of alginate.

3.2.2. *PCFC*

PCFC analysis allows getting complementary information on heat release. Fig. 3b shows the plots of the heat release rate (HRR, W g^{-1}) *vs.* temperature. The figure reports the data for FR-PUF and AF for anaerobic pyrolysis and for the aerobic pyrolysis of FR-PUF and AF residues.

The peak of HRR (pHRR) is reached at 334 °C for FR-PUF and does not exceed 82 W g^{-1}. Such value is much lower than those reported for a neat PU, based on methylene diphenyl isocyanate and 1,3-propane diol exhibiting two peaks of more than 200 and 150 W g^{-1} respectively at 330 and 440 °C (Benin, Gardelle, & Morgan, 2014). Alginate Foam is characterized by even lower HRR: the pHRR is observed 254 °C with a value as low as 18 W g^{-1}. This value makes alginate one of the FR-free organic materials with the lowest pHRR (Sonnier et al., 2016a; Walters & Lyon, 2003). The total heat release (THR) is deduced from the curves. In the case of Alginate Foam, the HRR values are so low that the integration of the data does not provide a meaningful value for THR (i.e., less than 3 kJ g^{-1}). The interest of AF is clearly appearing while

comparing with the THR of FR-PUF, which was around 15− 16 kJ g^{-1}, although this value is slightly lower than that reported for the neat PU mentioned above (22 kJ/g).

The heat of combustion is calculated as the ratio THR/mass loss fraction (measured using TGA). Based on the residue at 700 °C, the heat of combustion reaches 24.4 kJ g^{-1} for FR-PUF while it is down to 5 kJ g^{-1} for AF. The anaerobic pyrolysis of AF releases fuels with very low heat of combustion compared with FR-PUF. Figure AM5 compares the PCFC profiles for the anaerobic pyrolysis of AF with alginate powder and orange peel. Table AM1 (see AMS) compares the thermal characteristics of AF, alginate (in powder) and orange peels in order to evaluate the relative contributions of the organic load (orange peel) and alginate compound. A sharp (HRR: 37 W g^{-1}) peak at 251 °C characterizes the profile for alginate powder; which also shows smaller peaks or shoulders at 154, 308, 404 and 449 °C (maximum HRR close to 14 W g^{-1}). It is noteworthy that the broad band in the range 350− 530 °C is very close to the profile observed for AF. In the case of orange peel, the profile shows also great similarity in the range 430− 530 °C. However, a broad band is observed between 130 and 430 °C with 2 major peaks at 220 °C and 330 °C (with HRR close to 38 and 40 W g^{-1}, respectively), and an intermediary peak at 270− 275 °C (with HRR close to 32 W g^{-1}). These different peaks may be associated to the differentiated decomposition of compounds constitutive of orange peel: cellulose, hemicellulose, pectin and some highly combustible compounds such as essential oils, and terpenes, etc. The most intense peaks at 220 °C and 331 °C are consistent with TGA curves (Fig. 3a) and differential thermal gravimetry (not shown) and with previous characterizations of orange peel by Pathak et al. (2017). The PCFC profile (anaerobic conditions) of AF is a kind of convolution profile combining the contributions of alginate and orange peel (which are the most important fractions in the composite foam). These data tends to demonstrate that orange peel is the compound that contributes the most to the flammability of the composite: the THR of orange peel is close to 8 kJ g^{-1} (compared with less than 3 kJ g^{-1} for alginate powder). HRRs (in the range 30− 40 W g^{-1}) are relatively low, though higher than alginate powder over a wider range of temperature (200− 400 °C).

The residues are carbon-rich. Their decomposition may bring additional heat of combustion. To evaluate this potential, the residues were submitted to aerobic pyrolysis conditions using PCFC (Fig. 3b). The residues are effectively decomposed with relatively high HRRs. In the case of FR-PUF, decomposition begins at 300 °C, reaches a maximum at 515 °C (producing a HRR of 215 W g^{-1}) and finishes at 670 °C. The pHRR reaches 200 W g^{-1} while the THR is close to 35 kJ g^{-1}. It is noteworthy that the complete decomposition of the foam means that THR corresponds to heat of combustion. Alginate Foam exhibits a very different behavior. Indeed, the decomposition of the residue only shows two very intense and sharp peaks at 474 °C and 648 °C with high HRR values: 607 W g^{-1} and 472 W g^{-1}, respectively. Similar unexpected behavior was reported by Zhang et al. (2012): a sharp peak was observed at 429 °C for the aerobic pyrolysis of alginate-zinc fiber. The mechanism is not clearly explained and would deserve deeper studies. It is noteworthy that the replication of the test systematically showed similar two-peaks shape for the aerobic pyrolysis of residues though slight shifts of peak temperature were observed (by about 50 °C). The THR (and heat of combustion) is close to 10− 12 kJ g^{-1} (i.e., about one third of the value for FR-PUF).

The thermal decomposition of AF begins at lower temperature than FR-PUF but the release of heat of combustion is much lower. Despite similar percentages of residue under anaerobic pyrolysis conditions (i.e., close to 30%, at 700 °C), the residue of AF stores much less heat of combustion (released only when tested under aerobic pyrolysis conditions).

3.3. Fire properties at bench scale

3.3.1. UL94 test

Preliminary tests were inspired from UL94 V standard method for evaluating fire propagation. Foam pieces were cut at fixed dimensions (i.e., 12.7 cm × 1.3 cm), and exposed twice for 10 s to a burner. Figure AM6 compares the initial foam to triplicate tests for both FR-PUF and AF. Flame extinguishes immediately after the removal of the burner for the two materials and none of them shows dripping. It is noteworthy than AF maintains weak smoldering for 10−15 s; the material shrinks but the propagation of the burnt part of the foam is shorter than for FR-PUF. AF can be ranked as V0 or V1 material. Smoldering is a critical issue for many materials involved in fire propagation (Zammarano et al., 2016), especially for highly porous materials and bio-based supports (Moussa, Toong, & Garris, 1977; Palumbo, Lacasta, Navarro, Giraldo, & Lesar, 2017).

3.3.2. Rapaces

The foams were tested using RAPACES apparatus at different heat fluxes (i.e., 35, 50 and 75 kW m^{-2}) for 2-cm thick foam thickness; and for different thicknesses of AF foams (i.e., 1, 1.2, 1.7, 2.1 and 3 cm) exposed to a heat flux of 50 kW m^{-2}.

3.3.2.1. Effect of heat flux. Fig. 4 shows the HRR curves *vs.* time at different heat fluxes for FR-PUF and AF materials. Table 2 summarizes and compares the values of the different thermal parameters for FR-PUF and AF materials.

Fig. 4a,b shows that the curves are noisy; this is directly correlated to the low values of HRR. In addition, flame out occurs a few seconds after ignition in the case of AF, while more than 1 min is required for FR-PUF. This confirms the self-extinguishing behavior of AF, even at high heat flux. It is noteworthy that the heat of combustion is lower for FR-PUF measured on RAPACES than the value obtained with PCFC. This may be ascribed to flame inhibition due to FR additive. Figure AM2 shows that the foam contains up to 2.7% (wt. %) of chlorine and 0.7% (wt. %) of phosphorus (semi-quantitative data).

The values of EHC for FR-PUF are almost independent of heat flux: they vary between 6.8 and 6.4 kJ g^{-1}. They are non-negligible; therefore, the pyrolysis after ignition is enhanced not only by the heat flux from the cone but also by the heat feedback from the flame. EHC for AF is much lower but increases when heat flux increases (from 0.3 to 3.1 kJ g^{-1}). Indeed, when heat flux increases, a fraction of residue (which stores a high amount of heat, as proved by aerobic pyrolysis in PCFC) is decomposed by thermo-oxidation; therefore higher heat release can be measured. EHC values become closer to the PCFC data (i.e., 4−5 kJ g^{-1}) at high heat flux.

For FR-PUF, the heat flux hardly affects the residue, which is relatively low (between 27% and 22%). AF shows a very different trend: at high heat flux (i.e., 75 kW m^{-2}) the residue is of the same order of magnitude than for FR-PUF; on the opposite hand, at lower heat fluxes the residue reaches much higher values (i.e., between 70% and 61%). Figure AM7 shows the evolution of AF residue while increasing the heat flux: the material loses its solid structure only at the highest heat flux. These results show the remarkably higher stability of AF, at low-medium heat fluxes, than FR-PUF. The Alginate Foam also shows remarkably higher self-extinguishing properties (3−5 s) compared with FR-PUF (i.e., flame out at 74−93 s). This is another proof of the promising fire retardant properties of this biosourced foam. Figure AM8 shows pictures selected at remarkable steps (including flame extinction) in the RAPACES testing of FR-PUF and AF.

As expected, increasing the heat flux decreases the values of the time-to-ignition (TTI), which are relatively low for the two materials. It is noteworthy that AF exhibits little higher TTIs than the reference material (FR-PUF) (between50 % and 100% variation). Quintiere et al. (Schartel & Hull, 2007) proposed a series of equations (Eqs. 1–2) for

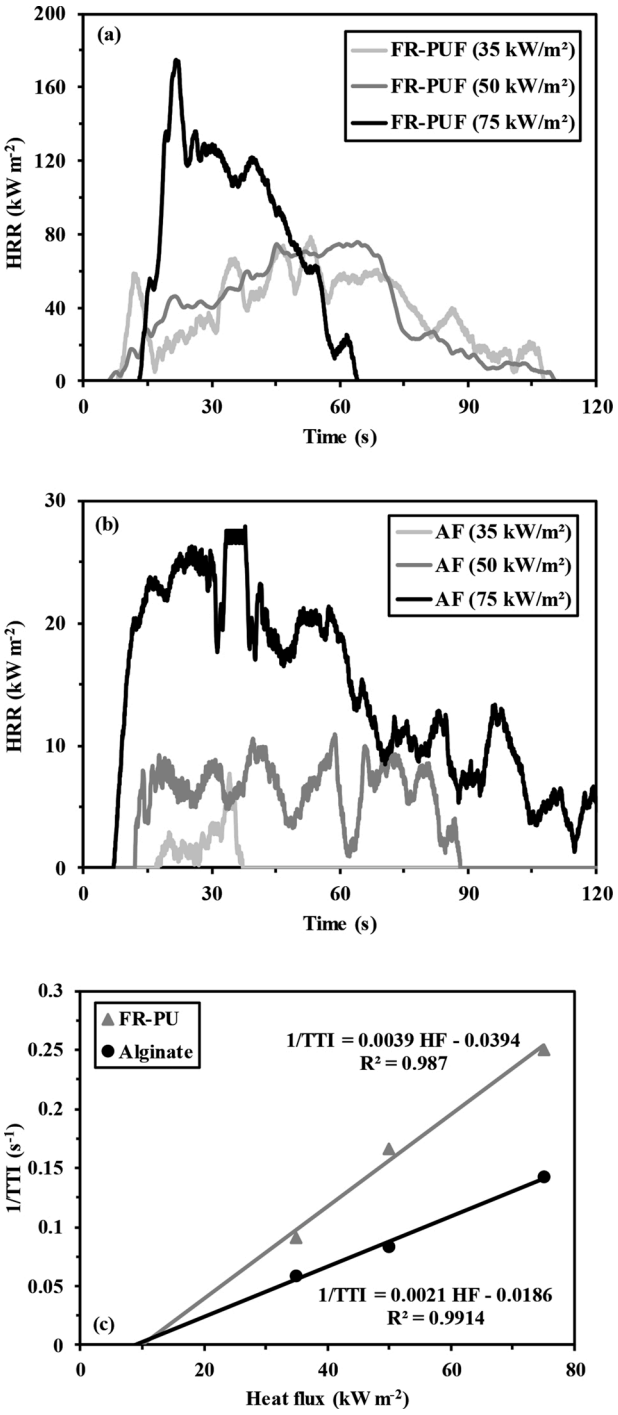

Fig. 4. RAPACES tests - HRR curves for FR-PUF (a) and AF (b) exposed to heat fluxes of 35, 50 and 75 kW m^{-2} and (c) effect of heat flux on the reciprocal of TTI for AF and FR-PUF.

predicting the ignition of thermally-thick and thermally-thin materials in cone calorimeter systems. Actually, the geometry of the RAPACES apparatus and the selected experimental conditions are analogous to those used for cone calorimeter system. This analogy allows applying this set of equations for RAPACES testing.

Thermally thick:

$$TTI = \frac{\pi}{4} K\rho C_p \left[\frac{T_{ig}-T_0}{\varepsilon \dot{q}''_{ext}-CHF}\right]^2 \quad (1)$$

Thermally thin:

$$TTI = l\rho C_p \frac{T_{ig}-T_0}{\varepsilon \dot{q}''_{ext}-CHF} \quad (2)$$

With K the heat conductivity (W m^{-1} K^{-1}), ρ the density, C_p the specific heat, T_{ig} the temperature at ignition (K), T_0 the room temperature (K), ε the emissivity, l the thickness; $\dot{q}''_{ext}$ is the external heat flux (kW m^{-2}) and CHF the critical heat flux (kW m^{-2}).

When the material is thermally thick, TTI depends on thermal conductivity because the heat transfer from the exposed surface to the bulk controls both the heating and the rate or relative proportion of pyrolysis zone. Considering the very low heat conductivity of foams, such phenomenon should be very limited. Therefore, the foams can be considered as thermally thin. The very low values of reported TTI (Table 2) confirm this interpretation. Moreover, for thermally thick behavior (Eq. 1), the curve $TTI^{-0.5}$ *vs.* heat flux should be linear. In addition, the extrapolation of the curve when $TTI^{0.5}$ tends to 0 corresponds to the critical heat flux (CHF; i.e., the minimum heat flux to provoke ignition). Here, CHF is found negative (not shown). On the contrary, for thermally thin behavior (Eq. 2), the curve TTI^{-1} *vs.* heat flux is expected linear. Fig. 4c shows the fit of experimental data derived from Eq. 2; the extrapolation for TTI^{-1} tending to 0 gives values close to 10 and 9 kW m^{-2} for FR-PU and alginate foams, respectively. Nevertheless, alginate is self-extinguishing (as discussed above), and flaming is not stable. In other words, critical heat flux for sustainable ignition should be much higher for alginate foam than for FR-PUF.

The peak of heat release rate (pHRR) is relatively weak for the two foams; however, it is 5–10 times higher for FR-PUF (80–170 kW m^{-2}) compared with AF (8–26 kW m^{-2}). For FR-PUF the THR is independent of the heat flux and close to 5 kJ g^{-1} while in the case of AF, the THR increases with heat flux. It is noteworthy that THR remains negligible (less than 0.6 kJ g^{-1}) until heat flux reaches 50 kW m^{-2}. Even at the highest heating flux (i.e., 75 kW m^{-2}) the THR of AF is 2 times lower than the value reported for FR-PUF.

3.3.2.2. Effect of AF thickness – Definition of the critical thickness (CT). In the case of materials subject to charring, the accumulation of the char strongly influences the heat transfer from the flame to the underlying surface. The heat transfer progressively decreases up to a limit depth, called here the critical thickness (CT). When the thickness of the burning material exceeds CT, flame extinction occurs. Obviously, this parameter is a key for designing protective coatings: when the coating thickness exceeds CT, the underlying material is not decomposed because the pyrolysis front is not reaching the surface of the protected object. In order to evaluate the CT value for composite AF, a series of blocks of different thicknesses was prepared (including the largest one; i.e., 3-cm thick, obtained by the assembly of three 1-cm thick blocks glued

Table 2
Main data in RAPACES for ≈2 cm-thick foams.

Foam	Heat flux (kW m^{-2})	Mass (g)	TTI (s)	pHRR (kW m^{-2})	THR (kJ g^{-1})	Residue (%)	EHC (kJ g^{-1})	Flame duration (s)
FR-PUF	35	8.4	11	80	5	27	6.8	74
	50	8.6	6	80	5	26	6.8	93
	75	8.9	4	170	5	22	6.4	76
AF	35	21.8	17	8	0.1	70	0.3	5
	50	23.2	12	17	0.6	61	1.5	3
	75	21.7	7	26	2.5	19	3.1	3

together with alginate-glue). It is noteworthy that for the multilayer block, the alginate layers are tightly bound (Figure AM3) and the contribution of the glue to heat release is negligible (not shown) because of the negligible amount of biopolymer and the proper fire properties of alginate. Due to the de-structuration of AF when exposed to 75 kW m^{-2} heat flux, it appears preferable evaluating this parameter under the irradiation of 50 kW m^{-2}. Indeed, the breaking of the char layer would affect the significance of observed protective effect.

Fig. 5 summarizes the plots of the HRR as a function of time for different thicknesses. Table 3 reports the main fire properties for AF blocks of different thicknesses. First, TTI occurs at only 6 s for the thinnest foam and 11− 12 s for the other samples, whichever the thickness. The HRR sharply increases to reach values as high as 40− 50 kW m^{-2} for the thinnest samples (i.e., 1 and 1.2 cm thick). After this peak (observed after 24− 27 s), the HRR progressively decreases to become negligible after 97− 117 s. On the opposite hand, for thicker samples (i.e., 1.7 cm and 2.1 cm) the HRR varies between 10 and 20 kW m^{-2}: the decrease of the HRR after the maximum is smoother than in the case of thin samples and the HRR maintains around 5 kW m^{-2} up to 88− 97 s. Surprisingly the 3-cm (multilayer) sample shows a higher HRR than intermediary samples; however, the signal is very noisy and the sharp initial peak of HRR rapidly decreases to a "standard" value close to the value obtained with the 2.1 cm thickness.

These different observations clearly demonstrate that the thickness is a key parameter for the protective effect of AF. For thicknesses below 1.7 cm, the pyrolysis front moves to the bottom of the sample and the entire foam volume is burnt. From 1.7 cm and above, the thickness exceeds the critical thickness, the pyrolysis front is stopped before reaching the sample bottom. It is important to keep in mind that radiation penetration is limited to a thin volume under the surface and heat conduction is negligible for foams (see above). Therefore, below 1.7-cm thickness, the whole volume of the foam is heated enough to pyrolyze: the residue is lower in percentage than the value reported for TGA (alginate is fully pyrolyzed and the char is partially decomposed by thermo-oxidation). Above 1.7 cm, a fraction of the foam remains unpyrolyzed: heat is not reaching this internal volume enough for decomposing the material. In this case, the residue represents a larger fraction than measured by TGA because it is a mix of char and unpyrolyzed foam; in addition, the THR (in kJ per g of initial material) decreases.

Moreover, the EHCs are close to the heat of combustion for 1 and 1.2 cm-thick (complete pyrolysis of the sample); they are slightly higher than reference values (i.e., <5 kJ g^{-1}) because a fraction of the char is thermo-oxidized. For higher thickness, the major difference is due to the mass loss associated with water release at low temperature (as explained below). These non-flammable gases decrease the value of EHC; they contribute to inhibit the combustion and promote fast flame-out (i.e., due to self-extinguishment). This is clearly confirmed by the drop in the flame duration (Table 2): stabilized in the range 30−23 s for the thinnest foams, it drastically decreases to 5−3 s for the thickest samples. The thinnest AF samples are not self-extinguishable: flame lasts for several dozens of seconds up to full pyrolysis. Actually, the flame may vanish; however, in some cases, re-ignition was observed. However, for thicknesses higher than CT the foams become self-extinguishable.

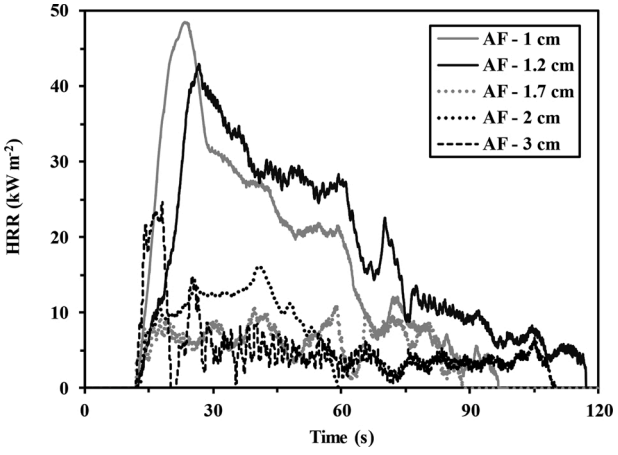

Fig. 5. HRR curves for AF with increasing thicknesses at 50 kW m^{-2} heat flux.

Table 3
Main data in RAPACES for different thicknesses of AF.

Thickness (cm)	Mass (g)	TTI (s)	pHRR (kW m^{-2})	THR (kJ g^{-1})	Residue (%)	EHC (kJ g^{-1})	Flame duration (s)
1.0	13.1	6	48	4.4	18	5.4	30
1.2	14.9	11	42	4.5	17	5.4	23
1.7	23.2	12	9	0.8	37	1.3	7
2.1	25.2	12	16	0.6	61	1.5	3
3.0[a]	53.4	12	21	0.4	84	1.0	3

[a] multilayer AF, in this specific test, the foam ignited for three seconds before extinguishing.

Figure AM9 compares the TTI values for the different foams: a clear breakthrough (slope change) is observed for thickness higher than 1.2 cm. While considering the flame duration (Figure AM10), the breakthrough is observed close to 1.7 cm thickness. Figure AM11 shows that the residue of combustion remains roughly constant (close to 18 %) up to a thickness of 1.2 cm and then continuously increases up to 84 % in the case of the multilayer AF (3 cm thickness). The critical thickness can be evaluated around 1.5–1.7 cm.

The self-extinguishable behavior of the thickest foams cannot be explained by the heat conduction, which would cool down the surface by transferring heat to the bulk (as reported above). Alternatively, it is possible suggesting that water release is involved in the self-extinguishment of thick foams. As already mentioned, in cone calorimeter fire tests (and also for RAPACES testing) the burning is one-dimensional (perpendicular to the surface). The AF are composite materials made of different compounds more or less complex: alginate, and orange peel (containing several polymers: cellulose, hemi-cellulose and pectins). Each component has a specific decomposition profile (depending on its proper thermal stability). Therefore, the decomposition front moves into the sample at a different rate for each component (Sonnier, Viretto, Dumazert, & Gallard, 2016). Water release occurs at lower temperature and it requires less heat than pyrolysis of alginate. Therefore, water is released from a larger volume than the pyrolyzed zone. Water acts as a diluent of gas phase: it decreases the EHC, and limits the flammability of this gas phase. Similar mechanisms have been reported for metal hydroxides such as alumina trihydrate and magnesium hydroxide (Hull, Witkowski, & Hollingbery, 2011). When the pyrolysis zone does not extend to the whole sample and is limited to critical thickness, the EHC decreases due to water release from an additional zone extending beyond the critical thickness.

To confirm that heat conduction is not controlling the fire behavior of AF, the surface temperature was recorded for the different foams (Fig. 6). The first sections of the curves are almost superimposed for the different systems. The temperature increases at the same rate up to around 300 °C (a in Fig. 6). This observation demonstrates that the heat transfer to the bulk does not contribute to decrease the heating rate of the surface during the pre-ignition step. Ignition temperature is relatively low but this is consistent with previous TGA and PCFC observations on alginate decomposition. After ignition, the surface temperature steeply increases up to 700 °C (between 632 and 738 °C): the maximum surface temperature (b in Fig. 6) tends to be much lower for thick foams. Very fast after reaching this maximum (after about 5 s), the temperature drastically drops; especially for thick foams. In the case of thermally-thin foams some secondary peaks are observed (c in Fig. 6); they are attributed to flame resumption. The glow that occurs in some cases facilitates the secondary burning phenomena while in the case of thick materials

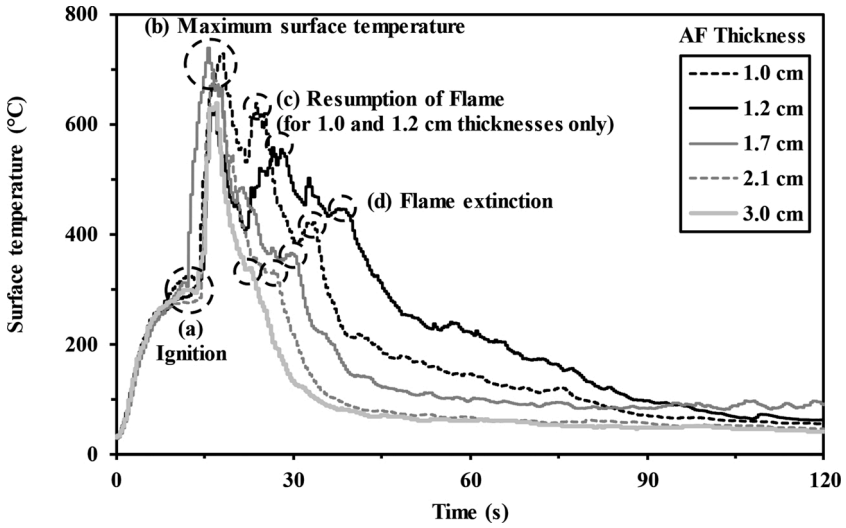

Fig. 6. Surface temperature of Alginate Foam with different thicknesses at 50 kW m^{-2} heat flow.

the water release from deepest layers could contribute to limit this phenomenon. Both the time (in the range 37−23 s) and the temperature of flame-out (in the range 440−330 °C) are decreasing with increasing the thickness of the foam (d in Fig. 6). It is noteworthy that the profiles do not show any plateau in the time course of surface temperature; this means that there is no-steady-state burning step in the global process.

3.4. *Effect of foam thickness on fire protection mechanism*

Fig. 7 shows a scheme summarizing and comparing the fire behavior of the AF foams depending on their thermally thin/thick characteristics. The main criteria driving the thermal degradation of the foams consist of:

a) Negligible heat conduction
b) Low heat of combustion
c) Charring formation
d) Water release

The crossed contributions of these different mechanisms may explain that for thicknesses higher than 1.5–1.7 cm the AFs are remarkably stable, with high production of residue, strong protection of underlying layers, and early flame-out.

3.5. *Comparison of fire properties for FR-RPU and AF*

Petrella (1994) suggested an arbitrary rating of materials on the basis of THR and flashover propensity (pHRR/TTI) (Table AM2). The commercial 2 mm-thick FR-PUF is systematically ranked as a *Low* THR-rated material (regardless of the heat flux). On the other hand for AF, for heat

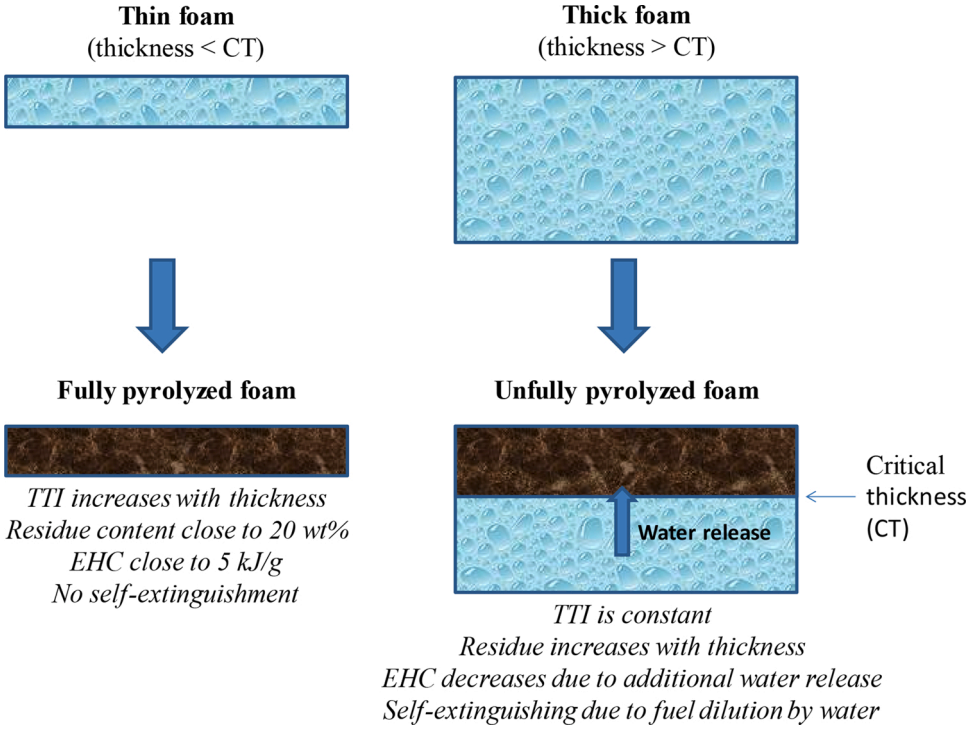

Fig. 7. Schematization of the effect of the thickness of AF on the fire protection.

flux between 25 and 50 kW m^{-2}, the material can be classified as *Very Low*; the material becomes *Low* THR-rated for 75 kw m^{-2} heat flux. However, even at high heat flux, the THR is halved compared with FR-PUF. Regarding the impact of the thickness, thermally-thin layers (1.0–1.2 cm thickness) have a *Low* THR-rating contrary to thermally-thick layers that are classified *Very Low* THR-rated materials. In terms of flashover propensity, FR-PUF is rated *Intermediate* at low heat flux (7.3 at 35 kW m^{-2}) but becomes *High*-rated at higher heat fluxes (13–43 at heat flux higher than 35 kW m^{-2}). The AF shows much lower flashover propensity: rated *Low* at 35 kW m^{-1}, and *Intermediate* at higher heat flux (i.e., 1.4–3.7).

The rating of flashover propensity also depends on the thickness of AF; at thickness lower than 1.7 cm the material is rated *Intermediate* (i.e., 3.7–3.8) while for thicker foams the material is classified *Low* (i.e., 0.75–1.33). The superior properties of AF compared with FR-PUF are confirmed, especially for foams having a thickness higher than the CT.

Another well-known parameter (i.e., FIGRA: flame index growth rate, kW m^{-2} s^{-1})) is also frequently used for evaluating and comparing the materials for fire protection. The lower is FIGRA, the lower is the fire hazard. Even if this parameter is highly dependent on some small peaks at low time (see Fig. 6), its value is much higher for FR-PU (2.3–8) than for AF (0.3–2.7, depending on the heat flux and the thickness).

3.6. Py-GC/MS analysis of gases emitted at 300 °C and 700 °C

Figure AM12 shows the Py-GC/MS chromatograms obtained for FR-PUF and AF samples pyrolyzed successively at 300 °C and 700 °C. Some of the produced compounds were identified by comparison with the NIST library and listed in Table AM3. The interpretation of the degradation patterns for FR-PUF is little easier since PUF materials have been extensively studied for their thermal degradation pathway. However, the type of precursors, blowing agents and fire retardant additives may strongly influence the products released during thermal degradation (Tang et al., 2002). The effective composition (and synthesis procedure) being confidential for the commercial FR-PUF, the complete identification of the peaks remains debatable. However, as generally described for PU materials, the release of isocyanate products is observed. A peak at 21.74 min attributed to 4,4′-methylenebis(phenyl isocyanate) is present for both 300 °C and 700 °C. This isocyanate product is widely used as cross-linker for formulation of PU systems. Moreover, complex compounds bearing P and Cl elements have been clearly identified, mainly at low temperature. The use of these chlorinated organophosphate products (products 17 and 18 - Table AM3) as FR for PU foams is well known. At high temperature, there is also production of various aromatic products, parts of which carry amine-bearing compounds like aniline or benzonitrile. In the case of composite alginate foam, few products have been detected for pyrolysis at 300 °C. The release of 2-methoxy-4-vinylphenol is attributed to the degradation of ferulic acid, which is generally present in orange peel. At high temperature, the presences of this orange peel (with a wide diversity of complex substances, meaning essential oil and so on), and alginate as the main constituents, make the identification of the peaks very complex (peak forest with very close retention times). However, most of these peaks correspond to aromatic products (including substituted phenols) conventionally formed during the pyrolysis of organic materials and already identified for alginate materials (Liu, Li, Zhao, Zhang, & Li, 2018; Ross et al., 2011). It is noteworthy that independent analyses carried out on pure alginate and orange peel (not shown) allowed identifying the origin of the compounds identified for retention times (14.2–14.3 min), assigned to compound 14 (i.e., 2-methoxy-4-vinylphenol) to the specific degradation of orange peel at 300 °C. At 700 °C, the gaseous products emitted by decomposition of the composite foam are almost the same as those produced with pure alginate: the other compounds present in the foam (including orange peel and other compounds, such as foaming agent) do not contribute to the degradation fingerprint of the foam at this temperature.

Commercial FR-PUF and AF exhibit very different degradation behavior with few degradation products in common. The release of halogenated products and isocyanates even at low pyrolysis temperature for the FR-PUF sample makes this kind of materials hazardous to health.

It is noteworthy that the thermal degradation of the composite foam (end-of-life or accidental burning) is much more environmentally friendly than conventional commercial foams, as revealed by PyGC/MS analyses. Fewer gases are produced and these gases are less hazardous than for commercial expanded foams. In addition, the foam is fully biodegradable (and naturally degradable in household compost bin within 4–6 weeks). The biodegradation of polystyrene is frequently estimated to several hundred years. While styrene can be biodegraded, the polymerization step strongly hinders the activity of microorganisms (Ho, Roberts, & Lucas, 2018). The degradation of polyurethane in compost is very slow: between 12% and 47% after 24 months (Krasowska, Heimowska, & Rutkowska, 2015).

3.7. Mechanical properties – compression tests

Compression tests (ISO 844 test for rigid cellular plastics) were performed on Alginate Foams with and without orange peel (the fire-retardant PUF tested for fire properties was also charcaterized) (Figure AM13). These results show that the two types of alginate-based foams have similar mechanical properties. Apparently, the incorporation of orange peel (AF) allowed reducing the variability in properties of mechanical resistance to compression compared with standard alginate foams (without orange peel). This hypothesis should be verified by more extensive tests. In addition, the mechanical characteristics, Young modulus and uniaxial stress at 10% strain, are increased by 6 and 18%, respectively. This enhancement should be considered as an indication due to the strong variation observed for AF peels without orange peel. The modulus is comparable for AF and FR-PUF materials while the uniaxial stress at 10% strain of AF is halved compared with the synthetic PUF. It is noteworthy that these materials have been designed for manufacturing environmentally friendly materials with enhanced fire retardant properties and insulating properties. The mechanical properties have been improved in other formulations (not documented in this work) by incorporation of natural fibers (cellulose, flax, etc.) (on-going work).

3.8. Foam stability

Time-stability has not been formally tested. This question is strongly dependent on the exposure conditions. However, materials kept inside (out of rain exposure) were stored for at least 2 years without significant degradation. Obviously, the material being essentially constituted of biopolymer and biomass, the foams are biodegradable. COD (950 mg O_2 L^{-1}) and BOD_{28} (900 mg O_2 L^{-1}) analyses were performed according the conventional methods (HACH and OXYTOP methods). The ratio DCO/BOD being close to 1.05, the material is considered highly biodegradable (comparable to cellulose). Non-normalized home-tests (not reported) were also performed to positively verify the backyard composting ability of these materials.

3.9. Water regain

The two foams show superposed curves for water regain within the first 9 h of exposure to humid atmosphere: the mass variation reaches $8.32 \pm 0.11\%$ (Figure AM14). A clear change in the rehydration profiles is observed above 9 h for the foams depending on the presence of peels. The incorporation of the orange peels contributes to a slightly higher water regain on the plateau reached after 24 h of exposure: $14.03 \pm 0.13\%$ vs. $12.67 \pm 0.01\%$. With increasing the exposure, the water regains stabilizes around $12.93 \pm 0.32\%$ for AF without peel, while for the reference material the water absorption continues to slightly increase (up to $14.67 \pm 0.65\%$ after 48 h). The presence of hygroscopic orange peel (pectines) contribute to a higher rehydration and

humidity storage; higher amplitudes are observed in water content for AF. This higher capacity to absorb water may contribute to enhanced fire retardant properties of the foams; through the effect of water release (according the mechanisms described in Fig. 7). The water content is higher than the value recorded for AF from TGA analysis; this is directly correlated to the high hygrometry for foam exposure (i.e., 75 ± 1 HR, %).

4. Conclusion

Innovative composite alginate foams were prepared by a simple proprietary process of foaming with incorporation of orange peels. These foams are characterized by irregular-shape closed cells; scaffolds delimitate large and heterogeneous-size cells (100−500 µm). The density of these foams can be readily adjusted to target values. The low heat conductivity of these materials make these materials highly promising as insulating coating in building industry. The flammability of this material was compared to the thermal behavior of a fire-retardant polyurethane foam. The composition of the composite AF was designed to assess materials of similar density (close to 40−42 kg m^{-3}). Alginate has unique properties as flame retardant. Indeed, the biopolymer readily chars and the char layer is cohesive (at least for heat flux not exceeding 50 kW m^{-2}, corresponding to the energy released by a fire in propagation). Moreover, alginate combustion releases very little amounts of heat, making fire propagation rather limited. The release of water from alginate foams acts as a diluent, which, in turn, contributes to fast flame-out.

Smoldering remains an important point to be solved, as occurring with many porous biosourced materials. Anyway, the UL 94 tests showed that AF has globally the same behavior as FR-PUF, and can be classified V0-V1 according to this standard.

The different methods used for characterizing the thermal properties of the materials (PCFC and RAPACES) demonstrate the superiority of Alginate Foams over FR-PUF, especially at heat flux not exceeding 50 kW m^{-2}; this is more specifically shown by much lower pHRR, THR, and EHC, much higher residue, and much shorter flame duration.

However, these fire retardant properties are strongly controlled by the thickness of the foam. A critical thickness was determined (for a heat flux of 50 kW m^{-2}) close to 1.5–1.7 cm for AF. Indeed, below this thickness the foam completely degrades. Above the critical thickness, the superficial layer tends to char, while the underlying layers release water that contributes to (a) diluting flammable gas, (b) reducing the heat of combustion; which, in turn, leads to enhanced flame-out. These conclusions have been confirmed by the analysis of surface temperatures, time-to-ignition, flame duration, and residue, using a newly-designed fire testing equipment (RAPACES). The propensity of alginate foams to water absorption (tests on water regain under controlled hygrometry) may contribute to these remarkable fire-retardant properties.

In addition, Py-GC–MS confirms that the gas produced from the combustion of the foams (at both 300 °C and 700 °C) are much less hazardous than those generated by polyurethane combustion under similar conditions. Taken also into account both the green-based composition of the foams and the biodegradation properties, these results show the promising perspectives opened by alginate-based materials for manufacturing light, thermal insulating foams with remarkable fire-retardant properties. Mechanical properties of AF are roughly comparable to FR-PUF in terms of compression tests.

CRediT authorship contribution statement

Thierry Vincent: Conceptualization, Investigation, Supervision. **Chloë Vincent:** Investigation, Methodology, Writing - original draft, Data curation. **Loïc Dumazert:** Formal analysis, Data curation. **Belkacem Otazaghine:** Formal analysis, Data curation. **Rodolphe Sonnier:** Methodology, Supervision, Writing - review & editing. **Eric Guibal:** Methodology, Writing - review & editing, Project administration.

Acknowledgements

The contributions of Alexandre Chéron, Jean-Claude Roux and Gwenn Le-Saout (from IMT-Mines Ales, C2MA) are acknowledged for mechanical tests, SEM and SEM-EDX analysis, and XRD characterization, respectively.

Appendix A. Supplementary data

Supplementary material related to this article can be found, in the online version, at doi:https://doi.org/10.1016/j.carbpol.2020.116910.

References

Li, Q. M., Wang, J. Y., Chen, L. M., Shi, H., & Hao, J. W. (2019a). Ammonium polyphosphate modified with beta-cyclodextrin crosslinking rigid polyurethane foam: Enhancing thermal stability and suppressing flame spread. *Polymer Degradation and Stability, 161*, 166–174.

Liu, Y., Wang, J.-S., Zhu, P., Zhao, J.-C., Zhang, C.-J., Guo, Y., et al. (2016a). Thermal degradation properties of biobased iron alginate film. *Journal of Analytical and Applied Pyrolysis, 119*, 87–96.

Liu, Y., Wang, J., Zhao, J., Zhang, C., Ran, J., & Zhu, P. (2014a). The flame retardancy and thermal degradation behaviors of trivalent metal-alginate films. *Nanomaterials and Energy, 3*(1), 3–10.

Sonnier, R., Otazaghine, B., Iftene, F., Negrell, C., David, G., & Howell, B. A. (2016a). Predicting the flammability of polymers from their chemical structure: An improved model based on group contributions. *Polymer, 86*, 42–55.

Agrawal, A., Kaur, R., & Walia, R. S. (2017). PU foam derived from renewable sources: Perspective on properties enhancement: An overview. *European Polymer Journal, 95*, 255–274.

Agulhon, P., Robitzer, M., Habas, J. P., & Quignard, F. (2014). Influence of both cation and alginate nature on the rheological behavior of transition metal alginate gels. *Carbohydrate Polymers, 112*, 525–531.

ASTM. (2013). *Test method for determining flammability characteristics of plastics and other solid materials using microscale combustion calorimetry, ASTM D7309. (Vol. ASTM D7309)*. West Conshohocken, PA, USA: American Society for Testing and Materials.

Li, X. L., Chen, M. J., & Chen, H. B. (2019b). Facile fabrication of mechanically-strong and flame retardant alginate/clay aerogels. *Composites Part B-Engineering, 164*, 18–25.

Liu, Y., Zhang, C.-J., Zhao, J.-C., Guo, Y., Zhu, P., & Wang, D.-Y. (2016b). Bio-based barium alginate film: Preparation, flame retardancy and thermal degradation behavior. *Carbohydrate Polymers, 139*, 106–114.

Liu, Y., Zhao, J., Zhang, C., Ji, H., & Zhu, P. (2014b). The flame retardancy, thermal properties, and degradation mechanism of zinc alginate films. *Journal of Macromolecular Science Part B-Physics, 53*(6), 1074–1089.

Sonnier, R., Viretto, A., Dumazert, L., & Gallard, B. (2016b). A method to study the two-step decomposition of binary blends in cone calorimeter. *Combustion and Flame, 169*, 1–10.

Benin, V., Gardelle, B., & Morgan, A. B. (2014). Heat release of polyurethanes containing potential flame retardants based on boron and phosphorus chemistries. *Polymer Degradation and Stability, 106*, 108–121.

BING. (2006). *Thermal insulation materials made of rigid polyurethane foam (PUR/PIR) / Properties - Manufacture. (p. 33)*. Brussels (Belgium): BING Federation of European Rigid Polyurethane Foam Associations.

Liu, Y., Zhao, J.-C., Zhang, C.-J., Guo, Y., Zhu, P., & Wang, D.-Y. (2016c). Effect of manganese and cobalt ions on flame retardancy and thermal degradation of bio-based alginate films. *Journal of Materials Science, 51*(2), 1052–1065.

Carosio, F., Ghanadpour, M., Alongi, J., & Wagberg, L. (2018). Layer-by-layer-assembled chitosan/phosphorylated cellulose nanofibrils as a bio-based and flame protecting nano-exoskeleton on PU foams. *Carbohydrate Polymers, 202*, 479–487.

Carosio, F., Negrell-Guirao, C., Alongi, J., David, G., & Camino, G. (2015). All-polymer Layer by Layer coating as efficient solution to polyurethane foam flame retardancy. *European Polymer Journal, 70*, 94–103.

Chen, M. J., Wang, X., Tao, M. C., Liu, X. Y., Liu, Z. G., Zhang, Y., et al. (2018). Full substitution of petroleum-based polyols by phosphorus-containing soy-based polyols for fabricating highly flame-retardant polyisocyanurate foams. *Polymer Degradation and Stability, 154*, 312–322.

Liu, Y., Zhao, X.-R., Peng, Y.-L., Wang, D., Yang, L., Peng, H., et al. (2016d). Effect of reactive time on flame retardancy and thermal degradation behavior of bio-based zinc alginate film. *Polymer Degradation and Stability, 127*, 20–31.

Delgado-Sanchez, C., Sarazin, J., Santiago-Medina, F. J., Fierro, V., Pizzi, A., Bourbigot, S., et al. (2018). Impact of the formulation of biosourced phenolic foams on their fire properties. *Polymer Degradation and Stability, 153*, 1–14.

Ding, H. Y., Huang, K., Li, S. H., Xu, L. N., Xia, J. L., & Li, M. (2017). Synthesis of a novel phosphorus and nitrogen-containing bio-based polyol and its application in flame retardant polyurethane foam. *Journal of Analytical and Applied Pyrolysis, 128*, 102–113.

Draget, K. I., SkjakBraek, G., & Smidsrod, O. (1997). Alginate based new materials. *International Journal of Biological Macromolecules, 21*(1-2), 47–55.

El Hage, R., Khalaf, Y., Lacoste, C., Nakhl, M., Lacroix, P., & Bergeret, A. (2019). A flame retarded chitosan binder for insulating miscanthus/recycled textile fibers reinforced biocomposites. *Journal of Applied Polymer Science, 136*(13).

Gady, O., Poirson, M., Vincent, T., Sonnier, R., & Guibal, E. (2016). Elaboration of light composite materials based on alginate and algal biomass for flame retardancy: Preliminary tests. *Journal of Materials Science, 51*(22), 10035–10047.

Grandviewresearch. (2019). In G. V. Research (Ed.), *Polymer foam Market size, share & trends analysis report By type (polyurethane, polystyrene, polyolefin, melamine, phenolic, PVC), By application, By region, and segment forecasts, 2019 - 2025* (Vol. 2019). Grand View Research.

Grasdalen, H., Larsen, B., & Smidsrod, O. (1977). ^{13}C-n.m.r. Studies of alginate. *Carbohydrate Research, 56*(2), C11–C15.

Grasdalen, H., Larsen, B., & Smidsrod, O. (1979). A p.m.r. Study of the composition and sequence of uronate residues in alginates. *Carbohydrate Research, 23*(1), 23–31.

Hamdani-Devarennes, S., El Hage, R., Dumazert, L., Sonnier, R., Ferry, L., Lopez-Cuesta, J. M., et al. (2016). Water-based flame retardant coating using nano-boehmite for expanded polystyrene (EPS) foam. *Progress in Organic Coatings, 99*, 32–46.

Ho, B. T., Roberts, T. K., & Lucas, S. (2018). An overview on biodegradation of polystyrene and modified polystyrene: The microbial approach. *Critical Reviews in Biotechnology, 38*(2), 308–320.

Hou, X. B., Xue, Z. X., & Xia, Y. Z. (2018). Preparation of a novel agar/sodium alginate fire-retardancy film. *Materials Letters, 233*, 274–277.

Huang, P. K., Wu, M. H., Pang, Y. Y., Shen, B., Wu, F., Lan, X. Q., et al. (2019). Ultrastrong, flexible and lightweight anisotropic polypropylene foams with superior flame retardancy. *Composites Part a-Applied Science and Manufacturing, 116*, 180–186.

Huggett, C. (1980). Estimation of rate of heat release by means of oxygen-consumption measurements. *Fire and Materials, 4*(2), 61–65.

Hull, T. R., Witkowski, A., & Hollingbery, L. (2011). Fire retardant action of mineral fillers. *Polymer Degradation and Stability, 96*(8), 1462–1469.

Jeon, O., Bouhadir, K. H., Mansour, J. M., & Alsberg, E. (2009). Photocrosslinked alginate hydrogels with tunable biodegradation rates and mechanical properties. *Biomaterials, 30*(14), 2724–2734.

Jones, M., Bhat, T., Kandare, E., Thomas, A., Joseph, P., Dekiwadia, C., et al. (2018). Thermal degradation and fire properties of fungal mycelium and mycelium - biomass composite materials. *Scientific Reports, 8*.

Jones, M., Mautner, A., Luenco, S., Bismarck, A., & John, S. (2020). Engineered mycelium composite construction materials from fungal biorefineries: A critical review. *Materials & Design, 187*, 16.

Kontoyannis, C. G., & Vagenas, N. V. (2000). Calcium carbonate phase analysis using XRD and FT-Raman spectroscopy. *Analyst, 125*(2), 251–255.

Krämer, R. H., Zammarano, M., Linteris, G. T., Gedde, U. W., & Gilman, J. W. (2010). Heat release and structural collapse of flexible polyurethane foam. *Polymer Degradation and Stability, 95*(6), 1115–1122.

Krasowska, K., Heimowska, A., & Rutkowska, M. (2015). Environmental degradability of polyurethanes. In C. Kumar Das (Ed.), *Thermoplastic elastomers - Synthesis and applications*. London (UK): IntechOpen.

Li, P., Wang, B., Liu, Y.-Y., Xu, Y.-J., Jiang, Z.-M., Dong, C.-H., et al. (2020). Fully bio-based coating from chitosan and phytate for fire-safety and antibacterial cotton fabrics. *Carbohydrate Polymers, 237*.

Liu, Z., Li, Z., Zhao, X., Zhang, L., & Li, Q. (2018). Highly efficient flame retardant hybrid composites based on calcium alginate/nano-calcium borate. *Polymers, 10*(6).

Liu, Y., Li, Z., Wang, J., Zhu, P., Zhao, J., Zhang, C., et al. (2015). Thermal degradation and pyrolysis behavior of aluminum alginate investigated by TG-FTIR-MS and Py-GC-MS. *Polymer Degradation and Stability, 118*, 59–68.

Liu, Y., Zhao, J.-C., Zhang, C.-J., Guo, Y., Cui, L., Zhu, P., et al. (2015). Bio-based nickel alginate and copper alginate films with excellent flame retardancy: Preparation, flammability and thermal degradation behavior. *RSC Advances, 5*(79), 64125–64137.

Lorenzetti, A., Besco, S., Hrelja, D., Roso, M., Gallo, E., Schartel, B., et al. (2013). Phosphinates and layered silicates in charring polymers: The flame retardancy action in polyurethane foams. *Polymer Degradation and Stability, 98*(11), 2366–2374.

Lyon, R. E., & Walters, R. N. (2004). Pyrolysis combustion flow calorimetry. *Journal of Analytical and Applied Pyrolysis, 71*(1), 27–46.

Mougel, C., Garnier, T., Cassagnau, P., & Sintes-Zydowicz, N. (2019). Phenolic foams: A review of mechanical properties, fire resistance and new trends in phenol substitution. *Polymer, 164*, 86–117.

Moussa, N. A., Toong, T. Y., & Garris, C. A. (1977). Mechanism of smoldering of cellulosic materials. *Symposium (International) on Combustion, 16*(1), 1447–1457.

Mu, X. W., Yuan, B. H., Pan, Y., Feng, X. M., Duan, L. J., Zong, R. W., et al. (2017). A single alpha-cobalt hydroxide/sodium alginate bilayer layer-by-layer assembly for conferring flame retardancy to flexible polyurethane foams. *Materials Chemistry and Physics, 191*, 52–61.

Palumbo, M., Lacasta, A. M., Navarro, A., Giraldo, M. P., & Lesar, B. (2017). Improvement of fire reaction and mould growth resistance of a new bio-based thermal insulation material. *Construction and Building Materials, 139*, 531–539.

Pan, Y., Liu, L. X., Cai, W., Hu, Y., Jiang, S. D., & Zhao, H. T. (2019). Effect of layer-by-layer self-assembled sepiolite-based nanocoating on flame retardant and smoke suppressant properties of flexible polyurethane foam. *Applied Clay Science, 168*, 230–236.

Pathak, P. D., Mandavgane, S. A., & Kulkarni, B. D. (2017). Fruit peel waste: Characterization and its potential uses. *Current Science, 113*(3), 444–454.

Petrella, R. V. (1994). The assessment of full-scale fire hazards from cone calorimeter data. *Journal of Fire Sciences, 12*(1), 14–43.

Qin, Y. M. (2008). Alginate fibres: An overview of the production processes and applications in wound management. *Polymer International, 57*(2), 171–180.

Rao, W. H., Xu, H. X., Xu, Y. J., Qi, M., Liao, W., Xu, S. M., et al. (2018). Persistently flame-retardant flexible polyurethane foams by a novel phosphorus-containing polyol. *Chemical Engineering Journal, 343*, 198–206.

Realinho, V., Haurie, L., Formosa, J., & Ignacio Velasco, J. (2018). Flame retardancy effect of combined ammonium polyphosphate and aluminium diethyl phosphinate in acrylonitrile-butadiene-styrene. *Polymer Degradation and Stability, 155*, 208–219.

Ross, A. B., Hall, C., Anastasakis, K., Westwood, A., Jones, J. M., & Crewe, R. J. (2011). Influence of cation on the pyrolysis and oxidation of alginates. *Journal of Analytical and Applied Pyrolysis, 91*(2), 344–351.

Safaei, M., Taran, M., & Imani, M. M. (2019). Preparation, structural characterization, thermal properties and antifungal activity of alginate-CuO bionanocomposite. *Materials Science & Engineering C-Materials for Biological Applications, 101*, 323–329.

Schartel, B., & Hull, T. R. (2007). Development of fire-retarded materials - Interpretation of cone calorimeter data. *Fire and Materials, 31*(5), 327–354.

Simkovic, I. (2013). Unexplored possibilities of all-polysaccharide composites. *Carbohydrate Polymers, 95*(2), 697–715.

Sui, K., Li, Y., Liu, R., Zhang, Y., Zhao, X., Liang, H., et al. (2012). Biocomposite fiber of calcium alginate/multi-walled carbon nanotubes with enhanced adsorption properties for ionic dyes. *Carbohydrate Polymers, 90*(1), 399–406.

Sun, X., Zhang, J., Ding, G., & You, Y. (2020). Tannin-based biosorbent encapsulated into calcium alginate beads for Cr(VI) removal. *Water Science & Technology, 81*(5), 936–948.

Tang, Z., Maroto-Valer, M. M., Andresen, J. M., Miller, J. W., Listemann, M. L., McDaniel, P. L., et al. (2002). Thermal degradation behavior of rigid polyurethane foams prepared with different fire retardant concentrations and blowing agents. *Polymer, 43*(24), 6471–6479.

Tian, H. F., Yao, Y. Y., Zhang, S., Wang, Y. R., & Xiang, A. M. (2018). Enhanced thermal stability and flame resistance of rigid polyurethane-imide foams by varying copolymer composition. *Polymer Testing, 67*, 68–74.

Torres, M. R., Sousa, A. P. A., Silva Filho, E. A. T., Melo, D. F., Feitosa, J. P. A., de Paula, R. C. M., et al. (2007). Extraction and physico-chemical characterization of *Sargassum vulgare* alginate from Brazil. *Carbohydrate Research, 342*(14), 2067–2074.

Vadas, D., Igricz, T., Sarazin, J., Bourbigot, S., Marosi, G., & Bocz, K. (2018). Flame retardancy of microcellular poly(lactic acid) foams prepared by supercritical CO_2-assisted extrusion. *Polymer Degradation and Stability, 153*, 100–108.

Vincent, C. (2016). *Caractérisation du comportement au feu des matériaux de l'habitat : Influence de l'effet d'échelle, PhD Thesis. IMT-Mines Alès, LGEI and C2MA (Vol. Ph.D.). Montpellier (France): Université de Montpellier*.

Vincent, C., Sabatini, F., Aprin, L., Longuet, C., Rambaud, G., Dusserre, G., et al. (2015). Multi-scale experiments of household materials burning. *Chemical Engineering Transactions, 43*, 2419–2424.

Vincent, T., Dumazert, L., Dufourg, L., Cucherat, C., Sonnier, R., & Guibal, E. (2018). New alginate foams: Box-Behnken design of their manufacturing; fire retardant and thermal insulating properties. *Journal of Applied Polymer Science, 135*(7).

Walters, R. N., & Lyon, R. E. (2003). Molar group contributions to polymer flammability. *Journal of Applied Polymer Science, 87*(3), 548–563.

Wang, Y., Kang, W. D., Chen, C., Zhang, X. Y., Yang, L. H., Chen, X., et al. (2019). Combustion behaviour and dominant shrinkage mechanism of flexible polyurethane foam in the cone calorimeter test. *Journal of Hazardous Materials, 365*, 395–404.

Wang, Y. T., Wang, F., Dong, Q. X., Xie, M. C., Liu, P., Ding, Y. F., et al. (2017). Core-shell expandable graphite @ aluminum hydroxide as a flame-retardant for rigid polyurethane foams. *Polymer Degradation and Stability, 146*, 267–276.

Wang, L. Y., Wang, C., Liu, P. W., Jing, Z. J., Ge, X. S., & Jiang, Y. J. (2018). The flame resistance properties of expandable polystyrene foams coated with a cheap and effective barrier layer. *Construction and Building Materials, 176*, 403–414.

Wang, S. X., Zhao, H. B., Rao, W. H., Huang, S. C., Wang, T., Liao, W., et al. (2018). Inherently flame-retardant rigid polyurethane foams with excellent thermal insulation and mechanical properties. *Polymer, 153*, 616–625.

Yang, J. C., Cao, Z. J., Wang, Y. Z., & Schiraldi, D. A. (2015). Ammonium polyphosphate-based nanocoating for melamine foam towards high flame retardancy and anti-shrinkage in fire. *Polymer, 66*, 86–93.

Yang, R., Wang, B., Han, X. F., Ma, B. B., & Li, J. C. (2017). Synthesis and characterization of flame retardant rigid polyurethane foam based on a reactive flame retardant containing phosphazene and cyclophosphonate. *Polymer Degradation and Stability, 144*, 62–69.

Yang, Y., Haurie, L., Wen, J., Zhang, S., Ollivier, A., & Wang, D.-Y. (2019). Effect of oxidized wood flour as functional filler on the mechanical, thermal and flame-retardant properties of polylactide biocomposites. *Industrial Crops and Products, 130*, 301–309.

Yang, Z., Yi, A.-h., Liu, J.-y., & Zhao, X. (2016). Study of fire hazard of flooring materials on data of cone calorimeter. In H. W. Yao (Ed.), *2015 International Conference on performance-based fire and fire protection engineering* (Vol. 135, pp. 584–587).

Zammarano, M., Cazzetta, V., Nazare, S., Shields, J. R., Kim, Y. S., Hoffman, K. M., et al. (2016). Smoldering and flame resistant textiles via conformal barrier formation. *Advanced Materials Interfaces, 3*(23).

Zhang, J., Ji, Q., Shen, X., Xia, Y., Tan, L., & Kong, Q. (2011). Pyrolysis products and thermal degradation mechanism of intrinsically flame-retardant calcium alginate fibre. *Polymer Degradation and Stability, 96*(5), 936–942.

Zhang, J., Ji, Q., Wang, F., Tan, L., & Xia, Y. (2012). Effects of divalent metal ions on the flame retardancy and pyrolysis products of alginate fibres. *Polymer Degradation and Stability, 97*(6), 1034–1040.

Zhang, M., Liu, X., Chen, Z., Wang, J., & Song, W. (2015). Experimental study of the heat flux effect on combustion characteristics of commonly exterior thermal insulation materials. In F. Changgen, & L. Shengcai (Eds.), *2014 International symposium on safety science and technology* (Vol. 84, pp. 578–585).

Zhang, M., Pan, H., Zhang, L. Q., Hu, L. H., & Zhou, Y. H. (2014). Study of the mechanical, thermal properties and flame retardancy of rigid polyurethane foams prepared from modified castor-oil-based polyols. *Industrial Crops and Products, 59*, 135–143.

Zhang, X. S., Xia, Y. Z., Yan, X., & Shi, M. W. (2018). Efficient suppression of flammability in flame retardant viscose fiber through incorporating with alginate fiber. *Materials Letters, 215*, 106–109.

Zhao, H. F., Nam, P. K. S., Richards, V. L., & Lekakh, S. N. (2019). Thermal decomposition studies of EPS foam, polyurethane foam, and epoxy resin (SLA) as patterns for investment casting; Analysis of hydrogen cyanide (HCN) from thermal degradation of polyurethane foam. *International Journal of Metalcasting, 13*(1), 18–25.